Journal of Rock Mechanics and Geotechnical Engineering 11 (2019) 760–769

Contents lists available at ScienceDirect

Journal of Rock Mechanics and Geotechnical Engineering

journal homepage: www.rockgeotech.org

Full Length Article

# A sand production prediction model for weak sandstone reservoir in Kazakhstan

Ainash Shabdirova [a,*], Nguyen Hop Minh [b], Yong Zhao [a]

[a] School of Engineering, Nazarbayev University, Astana, Kazakhstan
[b] Fulbright University Vietnam, Ho Chi Minh City, Viet Nam

ARTICLE INFO

*Article history:*
Received 31 July 2018
Received in revised form
10 October 2018
Accepted 13 December 2018
Available online 2 May 2019

*Keywords:*
Sand production
Shear failure
Perforation tunnel
Plastic zone
Weak sandstone

ABSTRACT

Weakly consolidated reservoirs are prone to sand production problem, which can lead to equipment damages and environmental issues. The conditions for sand production depend on stresses and properties of rock and fluid. Accurate sand volume estimation is, however, still a challenging issue, especially for reservoirs in weak formations. The weak reservoirs containing viscous or heavy oil are mainly discovered in shallow depths in Kazakhstan, with moderate temperature and pressure. Many prediction models developed for open-hole completions where the reservoir materials usually possess certain strength are not applicable for the local reservoirs where the materials are significantly weaker even if casing is used to support the wellbore with oil produced through the perforation tunnels. In this context, a prediction model was proposed where the volume of the produced sand was estimated as the volume of the plastic zone of the failed materials surrounding the perforation tunnels. The model assumes an evolving truncated conical shape for the damage zone and takes into account stress distributions and shear failure in this zone. Then, the proposed model was used to estimate sand volumes in 20 wells during oil production with sequential increase of flow rates. The predictions match well with the measured sand volumes in a local oil field. Finally, a sensitivity analysis was conducted on the model performance. It shows that the permeability of the plastic zone was the most significant controlling factor in the prediction results.



## 1. Introduction

Sand production is one of the major concerns associated with shallow heavy oil reservoirs. The produced sands generated can damage equipment which would not only increase the extraction cost, but also affect the production schedule. Furthermore, the produced sands should be treated and disposed properly to avoid environmental and ecological problems. The production conditions of weak sandstone reservoirs, for example in Kazakhstan, make the problem worse as oil is usually produced above the critical flow rate associated with sand production in order to achieve the target economic benefits. Unfortunately, sand production is frequently observed across several local oil fields. In this sense, although different sand control strategies had been applied, limited success was achieved as many wells had to be shut in for workover processes to clean up the tubing every two to three weeks. For effective management of the reservoir, a reliable and quick method to estimate the amount of sand produced beforehand is desirable.

There are two main stages in the sand production process. The first stage involves rock matrix failure while the second stage entails the detachment of sand grains and their transportation by fluid flow. Under the initial undisturbed condition, the intact formation will remain in its hydro–mechanical equilibrium state. Drilling and perforation of the formation would redistribute the stresses around the perforation tunnel. When the induced stress increases and exceeds the failure strength, rock matrix will fail during the drilling process. However, rock matrix failure may not always lead to sand production as disaggregated particles can still be held by capillary forces. These particles can be detached by the fluid at higher flow rate if the flow energy is sufficient to overcome the forces holding them together. Sand is produced through the erosion of these particles from the rock matrix.

Extensive research has been conducted to predict sanding onset based on the stress conditions at which failure occurs. There are

* Corresponding author.
*E-mail address:* ainash.shabdirova@nu.edu.kz (A. Shabdirova).
Peer review under responsibility of Institute of Rock and Soil Mechanics, Chinese Academy of Sciences.

https://doi.org/10.1016/j.jrmge.2018.12.015

two main failure mechanisms: tensile failure and shear failure (Fjær et al., 2008). Tensile failure occurs when effective principal stress $\sigma'$ in the rock exceeds its tensile strength $T_0$, which is mostly applicable in high-rate gas wells (Jin et al., 2011; Hayavi and Abdideh, 2017). The tensile failure criterion can be written as

$$\sigma' = -T_0 \tag{1}$$

Shear failure occurs when the tangential stress along the shear plane $\tau_{max}$ exceeds a critical value, which depends on the normal stress $\sigma'$:

$$|\tau_{max}| = f(\sigma') \tag{2}$$

Various failure criteria in terms of the function $f(\sigma')$ have been developed. For example, the Mohr-Coulomb, Mogi-Coulomb, Hoek-Brown, Drucker-Prager, and modified Lade failure criteria are used as the shear failure models for sanding onset (Bratli and Risnes, 1981; Risnes et al., 1982; Bradford and Cook, 1994; Yi et al., 2005; Nouri et al., 2006; Al-Shaaibi et al., 2013; Papamichos and Furui, 2013).

Unconfined compressive strength (UCS) is also used as a simple strength indicator of rocks in prediction of sanding onset (Nouri et al., 2006; Araujo-Guerrero et al., 2014), but it does not take into account the effect of confining stress and pore water pressure as the UCS is formulated in terms of total stress. The sanding onset condition is often specified in terms of critical drawdown, critical wellbore pressure or critical flow rate, which are the production conditions at which the failure criterion of the reservoir materials is fulfilled, leading to erosion of these materials.

As the stresses around the cavity increase, the material will transform from elastic to plastic state after failure. Bratli and Risnes (1981) identified a plastic zone of the failed materials around a cavity after shear failure. The work was extended by Risnes et al. (1982) by investigating the stresses around open borehole and cased-hole completions. It was found that the radius of plastic zone dramatically decreases for the cased boreholes. Following these works, the formation of plastic zone had been reported in several experimental and numerical studies (Tronvoll and Fjær, 1994; Goshtasbi et al., 2013). The shape of the plastic zone varies from circular to elliptical in cross-section, but it does not change along the borehole axis. To accurately predict sand production, it is necessary to determine the volume of the plastic zone and the discharge mechanism of the failed materials. Geilikman et al. (1994) developed a sand production model to predict sand production rate after well-startup for Canadian heavy oil reservoirs. The prediction model used the Drucker-Prager failure criterion and assumed erosion of a visco-plastic solid skeleton due to highly viscous fluid flow in a vertical wellbore with open-hole completion. The model did not consider the gravitational forces. van den Hoek and Geilikman (2003) generalized the model to derive the sand production rate for reservoirs of any strength and fluid viscosity. The model utilized the UCS of the plastic zone in the prediction. This model may not be suitable for weak sandstone reservoirs in Kazakhstan as the UCS value of intact formation is very low and can quickly drop to zero in the plastic state.

Gholami et al. (2016) developed an analytical model for sand prediction in a carbonate reservoir. The shape of the wellbore's cross-section was considered to change from circular to elliptical due to shear failure once the tangential stress at the vertex exceeds the critical value. The volume of the plastic zone of the failed materials was estimated using three different failure criteria: Mohr-Coulomb, Hoek-Brown, and Mogi-Coulomb, with the last providing the best match with field data. This model was used for open-hole completion and its applicability in weak reservoirs that are usually cemented and cased to maintain wellbore stability has yet to be determined.

Most of the existing prediction models consider open borehole and employ poro-elastoplastic model to find the stress distribution around the borehole. Once the borehole is cased and perforated, the stress distribution around the perforation will be different and this would affect the failure of the materials in this zone. Morita et al. (1989) presented a parametric study for perforation tunnel stability and formulated a cavity-failure envelope for the sanding onset condition.

The reservoir sandstones in the oilfield of Ustuyrt-Buzachi Sedimentary Basin in Kazakhstan are confined to shallow-marine sediments of Lower Cretaceous Age at 200–500 m depth. Deltaic depositional environment followed by sea transgression resulted in fine grains of reservoir rock and weak clay cement (Worden and Morad, 2003). The reservoir rock lithology varies with different proportions of quartz, feldspars and clay minerals. One of the main characteristics of the field is the high oil viscosity (200–800 mPa s). For vertical wells, the producing zone is cased and perforated with density of 16 shots per meter and phasing of 90°. The first fluid produced often contained perforation debris and possible additional failed sand materials. By assuming the perforation tunnel as an ideal circular pipe with dimensions obtained from the perforation gun passport, the volume of perforation debris can be estimated. The estimation of the volume of the failed materials needs further work as the initial sand burst is followed by reduction in sand production rate until steady state is achieved. In the steady state, the sand production can be zero for the given flow rate. Increasing production often triggers new surge of sand. In this context, we developed a prediction model to estimate the sand volume produced from weak sandstone reservoirs in Kazakhstan, where vertical wellbores are cased and oil is produced from horizontal perforations. In this model, stress conditions around a horizontal perforation tunnel are defined from the far-field stress condition of the reservoir. Combining with a failure criterion, the model determines the boundary conditions between the plastic zone of the failed rock and the elastic zone of the intact rock around a perforation tunnel. Perforation shape changes as the sand is produced from the plastic zone. The model assumes that the change of perforation dimensions would result in a long truncated conical shape similar to natural wormholes. Tremblay et al. (1999) studied the wormhole behavior during cold heavy oil production with sand (CHOPS) for unconsolidated sandstone reservoirs in Canada. The shape of the wormhole simulated in their laboratory study is presented in Fig. 1, which shows that the wormhole is enlarged towards the flow orifice. In this study, the wormhole shape of the perforation tunnel is assumed as a result of shear failure and stress distribution around the perforation. If the predicted results of the proposed model agree with field data, it would


**Fig. 1.** Shape of a wormhole simulated in the laboratory (Tremblay et al., 1999).

be a convenient tool to estimate the sand volume when the production condition changes at the site.

## 2. Development of a sand prediction model

### 2.1. Assumption

In the absence of major geological faults and impermeable shale layers, the reservoir rock can be assumed to be isotropic and homogeneous. In addition, the well is assumed to be in its infancy. In this early stage of the well development, water breakthrough can be ignored and it is reasonable to assume full oil saturation of the reservoir rock. As reservoir pressure is maintained by the injection wells in the oilfield, steady-state flow conditions are assumed. Furthermore, despite its simplicity, the Mohr-Coulomb failure criterion has been effectively used in many models for the sanding onset and it is also used herein. The assumptions in the model are summarized as follows:

(1) Isotropic and homogeneous materials;
(2) Full saturation;
(3) Mohr-Coulomb failure criterion; and
(4) Steady-state flow conditions.

### 2.2. Boundary conditions

In the local oilfield, the producing zone of the vertical well was cased and perforated with a density of 16 shots per meter and a phasing of 90°, which results in a 0.25 m vertical distance between two adjacent horizontal perforations. Fig. 2 shows a simplified boundary condition in the field with two horizontal perforation tunnels connected to a vertical wellbore. As the prediction model is developed for sanding prediction from one perforation tunnel, half of the vertical distance between the two tunnels is assumed as the outer radial boundary of the tunnel considered in the model, i.e. $R_o = 0.125$ m. The dimensions of the perforation tunnels can be estimated from perforation gun passport as follows: diameter $2R_i = 0.013$ m and length $L = 2$ m.

The wellbore radius is $r_w$. Each of the perforation tunnels is cylindrical in shape with initial radius $R_i$ and length $L$. The radial distance from the perforation axis $R$ can vary from $R_i$ to $R_o$. The distance along the perforation axis is $r$, where $r = r_w$ at wellbore wall and $r = r_w + L$ at perforation tip.

### 2.3. Pore pressure distribution around perforation tunnel

Fluid pressure profile along the perforation axis is given by Dake (1983) as follows:

$$p = p_{wf} + \frac{Q\mu}{2\pi kh}\left(\ln\frac{r}{r_w} + S\right) \tag{3}$$

where $p$ is the fluid pressure at distance $r$ from the wellbore wall; $p_{wf}$ is the fluid pressure on the wellbore wall; $Q$ is the well flow rate, $Q = qN$, in which $N$ is the number of perforations and $q$ is the flow rate from a single perforation; $\mu$ is the fluid viscosity; $k$ is the permeability of the reservoir; $h$ is the thickness of the producing zone; and $S$ is the skin factor.

The pore pressure profile obtained from Eq. (3) is shown in Fig. 3. On the cross-section plane perpendicular to the perforation axis, the pore pressure is assumed to be constant, the value of which depends on $r$, as given in Eq. (3). The pore pressure distribution is shown in the inset of Fig. 3.

### 2.4. Stress distribution and failure condition around the perforation tunnel

The poro-elastoplastic material model (Charlez, 1997) is employed to determine the stress distributions around the perforations. Stress transformation from a global to a local coordinate system for an inclined cylindrical cavity is shown in Fig. 4. The principal directions of the far-field stresses are given by the coordinate system $(x', y', z')$ whereas $(x, y, z)$ is the local coordinate system of the perforation tunnel and $z$ specifies the tunnel axis. The model considers a vertical wellbore with horizontal perforation tunnel aligned along the maximum horizontal stress $\sigma_H$ and hence we have $i = 90°$ and $a = 0°$, where $i$ and $a$ are the rotational angles from $(x', y', z')$ to $(x, y, z)$.

The local stress components $\sigma_x^o, \sigma_y^o, \sigma_z^o, \tau_{xy}^o, \tau_{yz}^o$ and $\tau_{zx}^o$ can be calculated from the far-field stress components $\sigma_H$, $\sigma_h$ and $\sigma_v$ using the following equations (Fjær et al., 2008):

$$l_{xx'} = \cos a \cos i \tag{4}$$

$$l_{yx'} = -\sin a \tag{5}$$

$$l_{zx'} = \cos a \sin i \tag{6}$$

$$l_{xy'} = \sin a \cos i \tag{7}$$

$$l_{yy'} = \cos a \tag{8}$$

$$l_{zy'} = \sin a \sin i \tag{9}$$

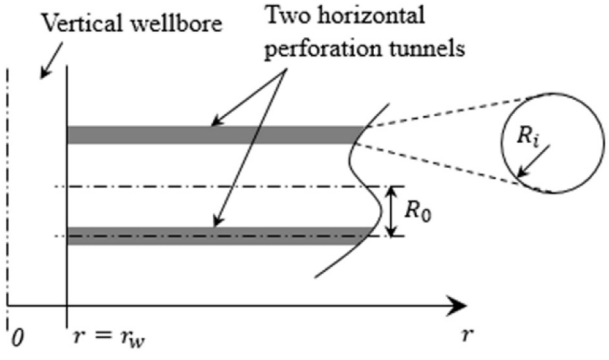


**Fig. 2.** Vertical wellbore with two horizontal perforation tunnels. The inset shows the enlarged circular cross-section of the tunnels.

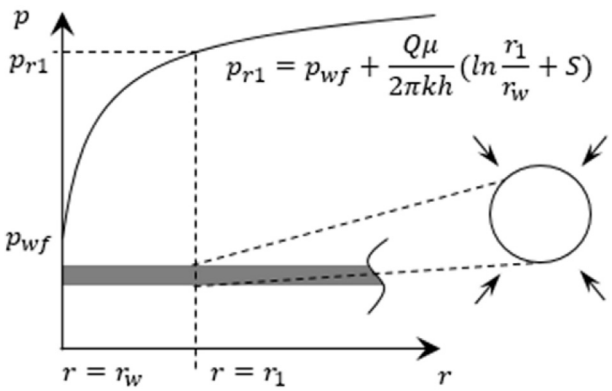


**Fig. 3.** Pore pressure profile along the perforation length and at cross-sections.

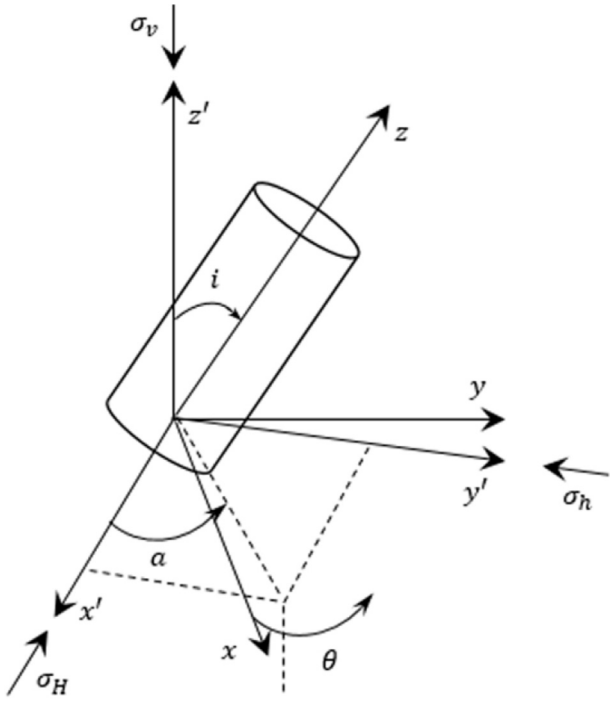


**Fig. 4.** Stress transformation with different coordinate systems (Fjær et al., 2008).

$$\sigma_x^o = l_{xx'}^2\sigma_H + l_{xy'}^2\sigma_h + l_{xz'}^2\sigma_v \tag{10}$$

$$\sigma_y^o = l_{yx'}^2\sigma_H + l_{yy'}^2\sigma_h + l_{yz'}^2\sigma_v \tag{11}$$

$$\sigma_z^o = l_{zx'}^2\sigma_H + l_{zy'}^2\sigma_h + l_{zz'}^2\sigma_v \tag{12}$$

$$\tau_{xy}^o = l_{xx'}l_{yx'}\sigma_H + l_{xy'}l_{yy'}\sigma_h + l_{xz'}l_{yz'}\sigma_v \tag{13}$$

The local stress components can then be used to calculate the cylindrical stress components distributed around the perforation tunnel where it is assumed that the materials next to the tunnel wall could be in a plastic state, whereas materials further away from the wall are in an elastic state (Risnes et al., 1982; Fjær et al., 2008). For the elastic zone, pore water pressure and flow properties are taken into account, whereas it is assumed that the materials in the plastic zone have failed and the stress conditions need to fulfill the failure condition in this region. Stresses in the elastic zone can be calculated as follows (Fjær et al., 2008):

$$\sigma_r = \frac{\sigma_x^o + \sigma_y^o}{2}\left(1 - \frac{R_i^2}{R^2}\right) + \frac{\sigma_x^o - \sigma_y^o}{2}\left(1 + 3\frac{R_i^4}{R^4} - 4\frac{R_i^2}{R^2}\right)\cos(2\theta) + \tau_{xy}^o\left(1 + 3\frac{R_i^4}{R^4} - 4\frac{R_i^2}{R^2}\right)\sin(2\theta) + p_{wf}\frac{R_i^2}{R^2} \tag{14}$$

$$\sigma_\theta = \frac{\sigma_x^o + \sigma_y^o}{2}\left(1 + \frac{R_i^2}{R^2}\right) - \frac{\sigma_x^o - \sigma_y^o}{2}\left(1 + 3\frac{R_i^4}{R^4}\right)\cos(2\theta) - \tau_{xy}^o\left(1 + 3\frac{R_i^4}{R^4}\right)\sin(2\theta) - p_{wf}\frac{R_i^2}{R^2} \tag{15}$$

$$\sigma_a = \sigma_z^o - \nu_{fr}\left[2\left(\sigma_x^o - \sigma_y^o\right)\frac{R_i^2}{R^2}\cos(2\theta) + 4\tau_{xy}^o\frac{R_i^2}{R^2}\sin(2\theta)\right] \tag{16}$$

where $\sigma_r$ is the radial stress at distance $R$ from the perforation axis, $\theta$ is the azimuth angle around the perforation axis, $\nu_{fr}$ is the Poisson's ratio, $\sigma_\theta$ is the tangential stress at distance $R$ from the perforation axis, and $\sigma_a$ is the axial stress at distance $R$ from the perforation axis.

For simplicity, the azimuth angle around the perforation axis is considered to be $\theta = 90°$ as stress variations for $0° \le \theta \le 180°$ are negligible due to small perforation radius compared to its length.

Stresses in the plastic zone can be determined as follows (Risnes et al., 1982):

$$\sigma_r = p_{wf} + \frac{\mu q}{2\pi L k_p}\ln\frac{R}{R_i} + \frac{1}{t}\left(2S_0\tan\alpha - \frac{\mu q}{2\pi L k_p}\right)\left[\left(\frac{R}{R_i}\right)^t - 1\right] \tag{17}$$

$$\sigma_\theta = p_{wf} + \frac{\mu q}{2\pi L k_p}\left(1 + \ln\frac{R}{R_i}\right) + \frac{1}{t}\left(2S_0\tan\alpha - \frac{\mu q}{2\pi L k_p}\right) \cdot \left[(t+1)\left(\frac{R}{R_i}\right)^t - 1\right] \tag{18}$$

$$\sigma_a = \sigma_\theta \tag{19}$$

where $q$ is the flow rate from a single perforation, $\mu$ is the fluid viscosity, $k_p$ is the permeability of plastic zone, $S_0$ is the inherent shear strength (cohesion), $\alpha$ is the failure angle, and $t = \tan^2\alpha - 1$.

The permeability in plastic zone, $k_p$, is generally not known, which is assumed to be less than that of the intact rock, $k$:

$$k_p = nk \tag{20}$$

In the current study, $k$ and $k_p$ can be estimated using the Kozeny-Carman equation (Eq. (21)), which depend on the particle diameter and material porosity. The values of the porosity for the intact material, $\phi$, and the failed material, $\phi_p$, can be obtained from the triaxial tests on the synthetic sandstone.

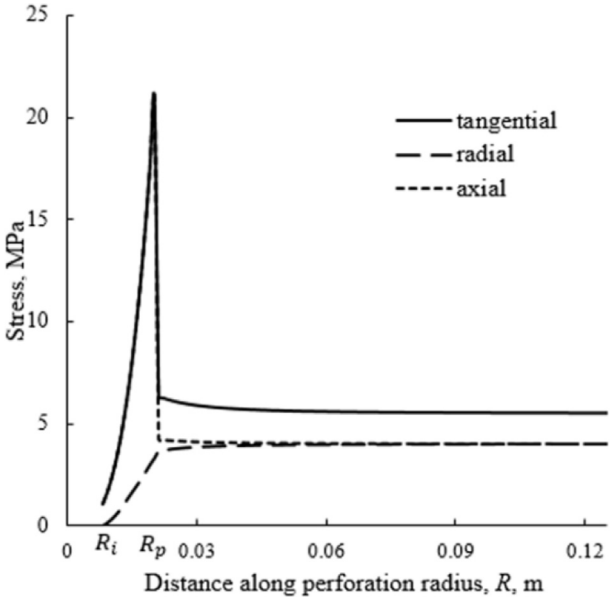


**Fig. 5.** Principal stresses around the perforation tunnel.

$$k = \frac{1}{180}\frac{\phi^3}{(1-\phi)^2}d_g^2 \tag{21}$$

where $d_g$ is the grain diameter. The relationship between the permeability of the intact rock, $k$, and the permeability of the plastic zone, $k_p$, can be derived from Eq. (21) as follows:

$$\frac{k}{k_p} = \frac{\phi^3\left(1-\phi_p\right)^2}{\phi_p^3(1-\phi)^2} = \frac{1}{n} \tag{22}$$

### 2.5. Plastic zone around the perforation tunnel

According to the model, the rock behaves elastically until the failure criterion is fulfilled in a form of shear failure. The Mohr-Coulomb failure criterion is used:

$$\sigma'_{1e} = 2S_0 \tan\alpha + \alpha'_{3p}\tan^2\alpha \tag{23}$$

where $\sigma'_{1e}$ is the effective maximum principal stress in the elastic zone, and $\sigma'_{3p}$ is the effective minimum principal stress in the plastic zone.

After failure, the rock reaches a plastic state, and the stress components in the failure criterion equation (Eq. (23)) are principal stresses. Fig. 5 shows that the radial stress is the minor principal stress and the tangential stress is the major principal stress in both plastic and elastic zones in the local oilfield in Kazakhstan. Further details of this field are discussed in the next section.

The failure criterion can be utilized to estimate the dimensions of the failed rock zone. Eq. (23) is rearranged as $\Sigma = S_0$, where the stress term $\Sigma = \sigma'_{1e}/(2\tan\alpha) - \sigma'_{3p}\tan\alpha/2$ is plotted in Fig. 6a and b. Two surfaces are plotted in Fig. 6a: the stress term $\Sigma = \sigma'_{1e}/(2\tan\alpha) - \sigma'_{3p}\tan\alpha/2$ and the rock strength $S_0$. For the region above the plane, the stresses are higher than the rock shear strength (i.e. $\sigma'_{1e}/(2\tan\alpha) - \sigma'_{3p}\tan\alpha/2 \geq S_0$) and failure occurs. The surfaces intersect to form a line $s$. Projection of the line $s$ onto the $L$-$R$ plane is shown in Fig. 6b, where $s'$ delineates the plastic zone borders. The radius of the plastic zone changes from $R_{p0}$ at the wellbore wall to $R_{pL}$ at the perforation tip. If the curved line $s'$ is replaced by a straight line (Fig. 7) for simplicity of calculation, the plastic zone around the perforation tunnel can be approximated by a truncated cone shape with $R_{p0} > R_{pL}$. Volume of the produced sand can be estimated from the volume of the truncated conical plastic zone.

Fig. 7 shows the cross-section of the plastic zone along the perforation tunnel, and Fig. 8 presents the plastic zone around the tunnel on the cross-section perpendicular to the tunnel axis. As the fluid enters the perforation from the reservoir and exits through the orifice to the wellbore, the radius of the plastic zone at the perforation tip, i.e. at the fluid inlet, $R_{pL}$, is less than the radius of the plastic zone at the orifice, $R_{p0}$. The model calculates two sand masses: $m_{perf}$ – the mass from the perforation tunnel (grey), and $m_p$ – the mass from the plastic zone (yellow). Example of sand volume calculation using the proposed model is given in Section 3.

## 3. Case study

### 3.1. Validation of the prediction model

Production data of a vertical well in Kazakhstan are used to calibrate the proposed prediction model. The well and field names are confidential, and will be referred to as Well 1 and Field X, respectively.

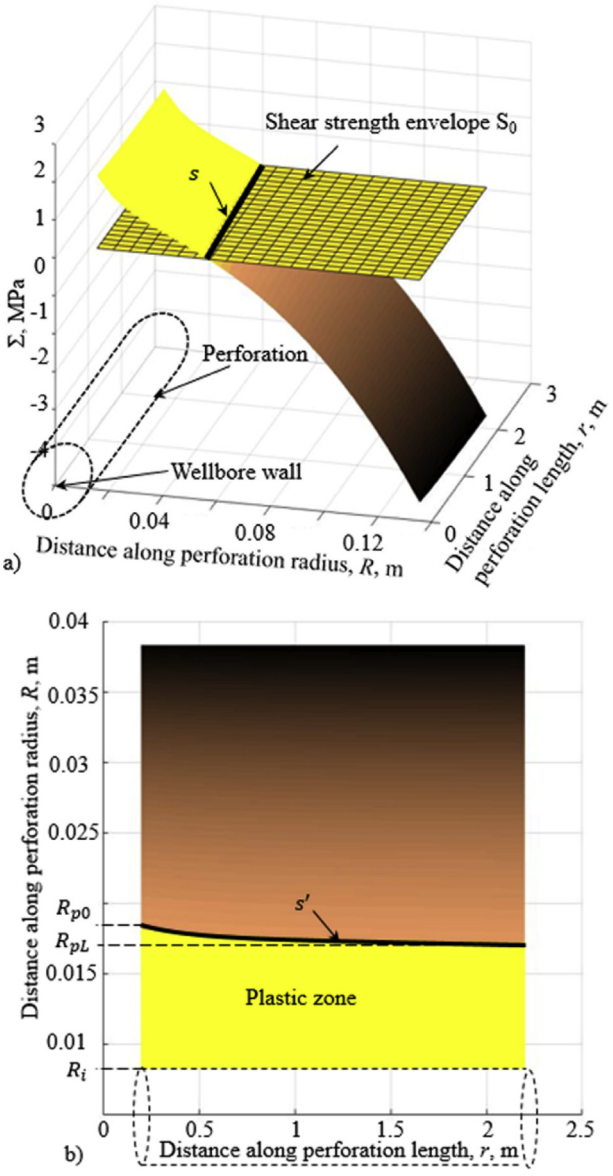


**Fig. 6.** Stresses around the perforation tunnel: (a) Three-dimensional view; and (b) Top view.

The effective thickness of the producing layer in Well 1 is 12 m at 277 m depth. Overburden gradient of 22.62 kPa/m results in the vertical stress $\sigma_v = 6.2$ MPa at the outer boundary of the perforation tunnel. Far-field horizontal stresses are assumed to be equal, i.e. $\sigma_H = \sigma_h = 4.7$ MPa. The initial reservoir pressure is 4 MPa, and the bottom-hole pressure is 0.7 MPa. The average porosity is 0.33, and the average permeability is 700 mD.

There is a lack of field data on the mechanical properties of the reservoir rock. The low strength of the material makes coring difficult and the quality of cored samples is very poor and cannot be

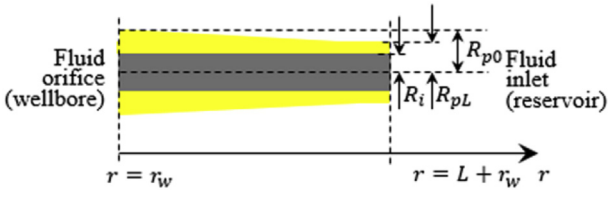


**Fig. 7.** Plastic zone along the perforation tunnel.

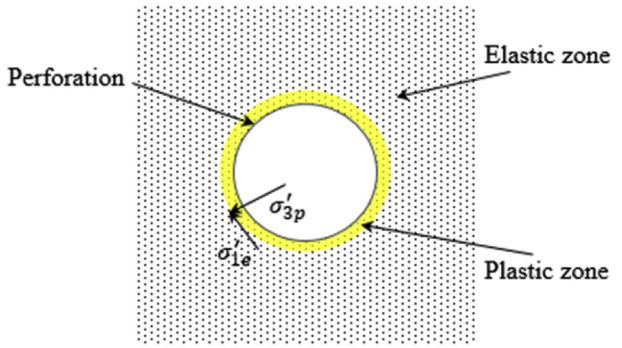


**Fig. 8.** Plastic zone on the perpendicular cross-section of the perforation tunnel.

used for direct mechanical testing. To address this problem, synthetic sandstones were prepared to replicate real reservoir rock in terms of composition, particle size distribution, and petrophysical properties. The porosity and permeability values of the synthetic sandstone are within the field data ranges. The mechanical properties of the failure angle, cohesion, and Poisson's ratio are determined from triaxial tests on the synthetic sandstone. Fig. 9 shows the Mohr-Coulomb failure envelope and the shape of sample at failure for the synthetic sandstone. The cohesion and failure angle of the synthetic sandstone agree with corresponding data of weak sandstones in the literature and are presented in Table 1.

Fig. 10 shows the porosity change in triaxial shearing of the synthetic sandstone. Assuming that the material is in intact state at the beginning and the plastic state starts as soon as the sample dilates, the values of $\phi$ and $\phi_p$ are found as 0.401 and 0.397, respectively, from the curve in Fig. 10, and $n = 0.95$. This value was applied to the reservoir permeability of 700 mD, and the plastic zone permeability was estimated as 665 mD.

The fluid flow rate and associated sand production for the period of the first 10 months of Well 1 are shown in Fig. 11. This well produces oil with water cut value below 0.05, and hence water presence is neglected and one phase flow is assumed. The field is characterized with heavy oil production with average fluid viscosity of 0.62 Pa s. The initial flow rate is around 200 bbl/d (Stage I, 1 bbl = 0.159 $m^3$), followed by more than double increase of 505 bbl/d (Stage II) at maximum. This production surge leads to a burst of sand. The next small rise of flow rate (Stage III) results in some additional sand production. Further fluctuation of fluid production below the maximum value did not trigger new sand burst, and sand production declined with time. As the model only considers a single perforation, the total flow rate is divided by the number of perforations in order to calculate the fluid flow rate from one perforation. Table 1 summarizes all the input data.

### 3.2. Sand prediction for Stage I

Prediction of the sand production for Stage I was conducted according to the following procedures:

(1) Step 1. The sand mass from the perforation tunnels is calculated as follows:

$$m_{perf} = \pi R_i^2 L \rho_s (1-\phi) N = 139 \text{ kg}$$

(2) Step 2. Using Eqs. (15) and (17), the effective tangential stresses $\sigma'_{\theta e}$ in the elastic zone and the effective radial stresses $\sigma'_{rp}$ in the plastic zone are calculated at various radial distances around the perforation tunnel. Distribution of $\sigma'_{\theta e}$ and $\sigma'_{rp}$ will also change along the perforation longitudinal length as the pore pressure changes. The values of the radial distance at which $\sigma'_{\theta e}$ and $\sigma'_{rp}$ satisfy Eq. (23) at each cross-section along the tunnel longitudinal axis can be found. These radial values correspond to the radii of plastic zone $R_p$ along the perforation tunnel. For example, the radius of plastic zone changes from $R^I_{p0} = 0.0186$ m at the borehole wall to $R^I_{pL}$=0.0177 m at the perforation tip. Assuming that the plastic zone forms a truncated cone with the larger and smaller radii equal to $R^I_{p0}$ and $R^I_{pL}$, respectively, the mass of sand produced from the plastic zone at $q_1 = 2$ cm for Stage I can be determined:

$$m^I_p = \left\{ \frac{\pi}{3}\left[ \left(R^I_{p0}\right)^2 + R^I_{p0}R^I_{pL} + \left(R^I_{pL}\right)^2 \right] L - \pi R_i^2 L \right\} \rho_s (1-\phi) N = 527 \text{ kg}$$

(3) Step 3. The theoretical total sand mass is obtained:

$$m^I_{total} = m_{perf} + m^I_p = 666 \text{ kg}$$

(4) Step 4. The theoretically predicted sand mass was compared with the sand mass obtained from field data, i.e. $m^I_{rf}$=639 kg. The findings indicated that in the first stage, the model overestimates the sand production by 4%, and for the current flow rate, the sand production is still ongoing, i.e. not all the sand from the plastic zone is produced.

### 3.3. Sand prediction for Stages II and III

Steps 2–4 in the Section 2 are repeated for the increased flow rate. For $q_2 = 4.6$ $cm^3/s$, the plastic zone extends from $R^{II}_{p0} = 0.0291$ m to $R^{II}_{pL} = 0.025$ m. The sand mass produced from the plastic zone at Stage II can now be calculated as

$$m^{II}_p = \left\{ \frac{\pi}{3}\left[ \left(R^{II}_{p0}\right)^2 + R^{II}_{p0}R^{II}_{pL} + \left(R^{II}_{pL}\right)^2 \right] L - \frac{\pi}{3}\left[ \left(R^{I}_{p0}\right)^2 + R^{I}_{p0}R^{I}_{pL} + \left(R^{I}_{pL}\right)^2 \right] L \right\} \rho (1-\phi) N = 815 \text{ kg}$$

If we assume that the remaining sand from Stage I, which can be calculated as a difference between the total sand mass and real sand mass for Stage I ($m^I_{total} - m^I_{rf} = 666$ kg $-639$ kg), is also produced with the increased flow rate, the total sand mass for Stage II will be

$$m^{II}_{total} = m^{II}_p + \left( m^I_{total} - m^I_{rf} \right) = 842 \text{ kg}$$

Similarly, for $q_3 = 4.9$ $cm^3/s$, the plastic zone extends from $R^{III}_{p0} = 0.031$ m to $R^{III}_{pL} = 0.0266$ m. In this stage, the mass of produced sand is calculated as

$$m^{III}_p = \left\{ \frac{\pi}{3}\left[ \left(R^{III}_{p0}\right)^2 + R^{III}_{p0}R^{III}_{pL} + \left(R^{III}_{pL}\right)^2 \right] L - \frac{\pi}{3}\left[ \left(R^{II}_{p0}\right)^2 + R^{II}_{p0}R^{II}_{pL} + \left(R^{II}_{pL}\right)^2 \right] L \right\} \rho_s (1-\phi) N = 198 \text{ kg}$$

All the calculated results are summarized in Table 2.

Table 2 shows that the proposed model predicts the sand productions in Stages I and II relatively well. High error in the third stage

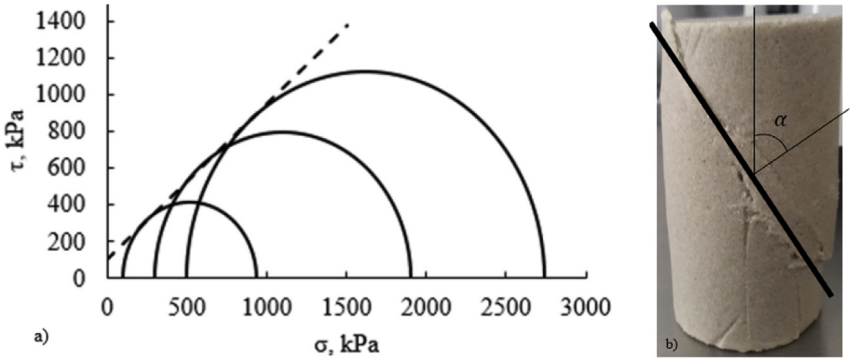


**Fig. 9.** Cohesion and failure angle of synthetic sandstone: (a) Mohr-Coulomb failure envelope; and (b) Failed sample.

can be due to the expected significant changes in material strength and other input parameters that are not considered in this study.

Similar procedure was conducted for 19 more wells in the same field. Ranges of main characteristics of the wells are shown in Table 3.

Fig. 12 shows the prediction performances for all the 20 wells. The model can predict the sand produced from 10 wells in Stage I within a maximum error of ±5% and 8 wells in Stage II within a maximum error of ±5%. Six wells in the first two stages have higher prediction errors of ±50% and these wells are associated with deeper producing horizons. The model has difficulties in predicting the sand volume produced in Stage III. In the third stage, only three wells can be adequately predicted with the error within 20%. For the rest of the 17 wells in the third stage, the prediction errors are higher (at ±50%). This may be due to the fact that the rock properties in Stage III may have deteriorated and are no longer constant. The increase in the water cut level in Stage III might also contribute to the estimation errors.

## 4. Sensitivity analysis of the prediction model

The proposed model is simple, but not all input data are known or available. Values determined from laboratory experiments may not always represent the real reservoir rock. Perforation dimensions were estimated based on the perforation gun passport information. In addition, oil viscosity was determined at the surface and converted to bottom-hole conditions. The fluid viscosity can vary slightly from well to well. All these add uncertainties to the accuracy of the input parameters, and their effect on the model performance should be studied.

Investigation on the influence of 6 parameters when varying each parameter value between 2 levels would result in $2^6 = 64$ cases. In order to reduce the number of cases and at the same time to keep the efficiency of the analysis, Taguchi method (Taguchi and Rafanelli, 1993) is used. The method produces an orthogonal array of cases with varying levels of each parameter. Factors selected for analysis and their boundary values are shown in Table 4.

Fractional factorial design, developed by the Taguchi method, for five parameters with two levels results in 8 cases, as tabulated in Table 5. Level 1 corresponds to the values 50% less than the baseline and level 2 corresponds to the values 50% more than the baseline for all parameters. Sand volume during Stage I for each case is calculated based on the proposed method. The resulting sand volume for each of the 8 cases is shown in Table 5.

Table 6 shows the range analysis. For each parameter, $K_1$ represents the amount of sand mass that could be produced under the effect of level 1 of that input while the other inputs are varied in different combinations, as shown in Table 5. Similarly, $K_2$ represents the amount of sand mass that could be produced under the effect of level 2 of the same input. Taking the parameter $L$ as an example, the $K_1$ value is calculated based on the average sand mass produced in cases 1–4, while $K_2$ is based on the average sand mass of cases 5–8. The range value $D$ for each parameter is calculated as the ratio between the larger $K$ to the smaller $K$ value between the two levels. $D$ is used to quantify the sensitivity of the parameter to the sand mass, where higher $D$ value shows that the input parameter possesses a stronger influence on the output results and vice versa.

On the basis of the sensitivity analysis results, it can be concluded that the initial perforation dimensions and rock and fluid properties with $D$ values less than 2 have moderate impact on the model performance. By contrast, the permeability of the plastic zone is shown to be the most influential factor with its $D$ value of about 4.6.

The permeability of the plastic zone should depend on the porosity and size distribution of the particles in the plastic zone and these in turn depend on the local volume change and eroded particles, which are subjected to flow dynamics. This phenomenon is highly complex and is not considered in this study.

## 5. Discussion

The sand prediction results of the 20 different wells show that the model best predicts the sand production if the reservoir depth does not exceed 280 m. The oilfield reservoirs are confined to three main producing horizons with the maximum depths of the first, second and third horizons as 280 m, 340 m, and 490 m, respectively. It is expected that the strength and porosity of the formation will vary with depth. On the other hand, single values of the strength parameter $S_0$ and the formation permeability $k$ ($k_p$) were used in the proposed model. The model overestimated sand production for deeper wells, which are not supported by the field data observed for those wells. This overestimation of the sand production at greater depth could be due to the underestimation of the shear strength and overestimation of the hydraulic conductivity assumed in the model.

For the 20 wells, we observed different formation lithologies from pure sandstone layers to complex interbedded layers of sandstone, shale, mudstone, siltstone and other minerals. However, the model assumes homogeneous and isotropic rock with single values of $\phi$ and $k$. As such, it cannot model the complex fluid flow through the interbedded layers. The unaccounted uncertainty in porosity and secondary permeability could attribute to the prediction inaccuracy. The prediction accuracy is further affected by the assumption of a constant flow rate with the steady-state flow

**Table 1**
Reservoir and production data.

| Item | Parameter | Stage I | Stage II | Stage III |
|---|---|---|---|---|
| Pressures | Fluid pressure at outer boundary, $p_o$ (MPa) | 4 | 4 | 4 |
| | Fluid pressure at borehole, $p_w$ (MPa) | 3 | 2.1 | 2.6 |
| | Vertical stress at boundary, $\sigma_v$ (MPa) | 6.2 | 6.2 | 6.2 |
| | Maximum and minimum horizontal stresses at boundary, $\sigma_H = \sigma_h$ (MPa) | 4.7 | 4.7 | 4.7 |
| Perforation dimensions | Perforation radius, $R_i$ (m) | 0.0083 | 0.0083 | 0.0083 |
| | Perforation length, $L$ (m) | 2 | 2 | 2 |
| | Radius of outer boundary, $R_o$ (m) | 0.125 | 0.125 | 0.125 |
| | Number of perforations, $N$ | 192 | 192 | 192 |
| Rock properties | Permeability, $k$ (D) | 0.7 | 0.7 | 0.7 |
| | Porosity, $\phi$ | 0.33 | 0.33 | 0.33 |
| | Poisson's ratio, $\nu$ | 0.45 | 0.45 | 0.45 |
| | Compressibility ratio, $\eta$ | 0.1 | 0.1 | 0.1 |
| | Cohesion, $S_0$ (MPa) | 0.1 | 0.1 | 0.1 |
| | Failure angle, $\alpha$ (°) | 63 | 63 | 63 |
| | Grain density, $\rho_s$ (kg/m$^3$) | 2500 | 2500 | 2500 |
| Plastic zone parameter | Minimum permeability in plastic zone (D) | 0.665 | 0.665 | 0.665 |
| Fluid properties | Fluid rate (cm$^3$/s) | 2 | 4.6 | 4.9 |
| | Fluid viscosity (Pa s) | 0.62 | 0.62 | 0.62 |

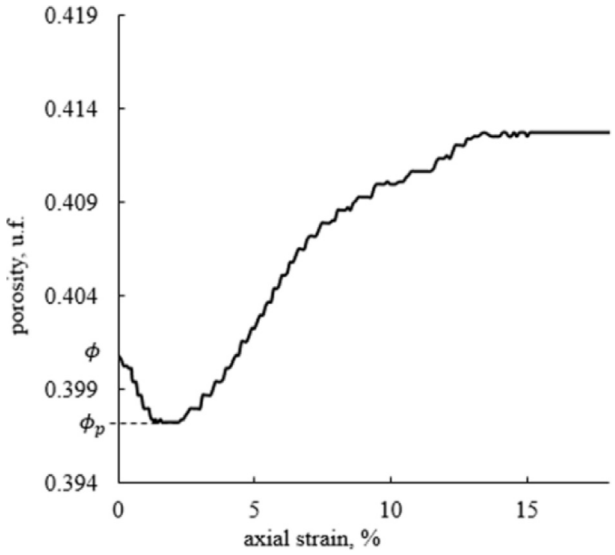


**Fig. 10.** Porosity change in triaxial shearing of synthetic sandstone.

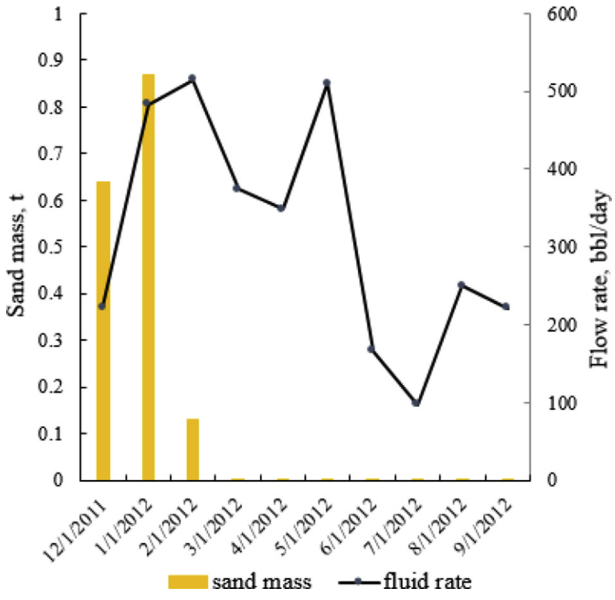


**Fig. 11.** Production data.

condition and it does not take into account the complex transition between different flow regimes in an actual production process of a well.

**Table 2**
Results of sand prediction model for Well 1.

| Stage | $q$ (cm$^3$/s) | $R_i$ (m) | $R_{p0}$ (m) | $R_{pL}$ (m) | $m_{rf}$ (kg) | $m_{total}$ (kg) | Error (%) |
|---|---|---|---|---|---|---|---|
| I | 2 | 0.0083 | 0.0186 | 0.0177 | 639 | 666 | 4 |
| II | 4.6 | 0.0083 | 0.0291 | 0.025 | 870 | 842 | −3 |
| III | 4.9 | 0.0083 | 0.0252 | 0.0328 | 131 | 198 | 51 |

**Table 3**
Ranges of characteristics for wells.

| Reservoir depth (m) | Producing zone thickness (m) | Flow rate (from a single perforation) (cm$^3$/s) | Water cut value (%) |
|---|---|---|---|
| 150–640 | 5–33 | 0.3–28 | 0–40 |

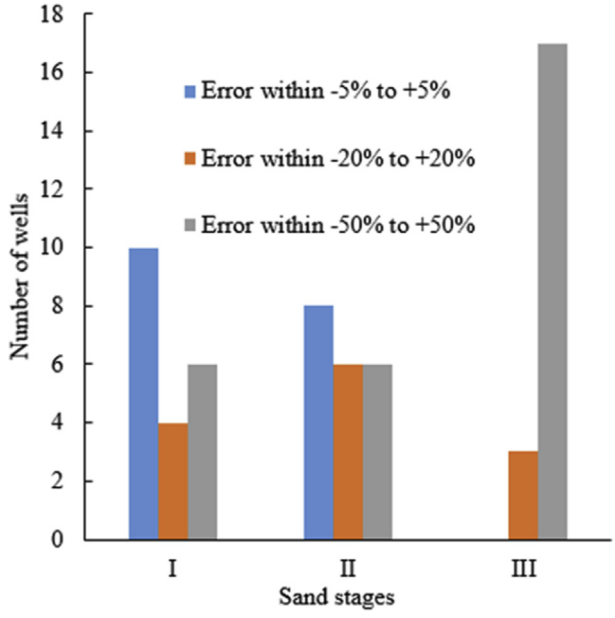


**Fig. 12.** Sand predictions in three stages for different wells.

**Table 4**
Parameters for sensitivity analysis.

| Case | Perforation length, $L$ (m) | Perforation radius, $R_i$ (m) | Permeability of plastic zone, $k_p$ (D) | Cohesion, $S_0$ (MPa) | Fluid viscosity (Pa s) |
|---|---|---|---|---|---|
| Baseline | 2 | 0.0083 | 0.665 | 0.12 | 0.62 |
| Level 1 (−50%) | 1 | 0.00415 | 0.35 | 0.06 | 0.31 |
| Level 2 (50%) | 3 | 0.01245 | 1.05 | 0.18 | 0.93 |

**Table 5**
Cases for sensitivity analysis.

| Case | $L$ | $R_i$ | $k_p$ | $S_0$ | $\mu$ | Sand mass (t) |
|---|---|---|---|---|---|---|
| 1 | Level 1 | Level 1 | Level 1 | Level 1 | Level 1 | 15.9 |
| 2 | Level 1 | Level 1 | Level 1 | Level 2 | Level 2 | 15.9 |
| 3 | Level 1 | Level 2 | Level 2 | Level 1 | Level 1 | 1.3 |
| 4 | Level 1 | Level 2 | Level 2 | Level 2 | Level 2 | 0.6 |
| 5 | Level 2 | Level 1 | Level 2 | Level 1 | Level 2 | 0.5 |
| 6 | Level 2 | Level 1 | Level 2 | Level 2 | Level 1 | 0.3 |
| 7 | Level 2 | Level 2 | Level 1 | Level 1 | Level 2 | 15.9 |
| 8 | Level 2 | Level 2 | Level 1 | Level 2 | Level 1 | 1.3 |

**Table 6**
Range analysis for sand volume.

| Parameters | Sand mass (t) | | $D$ |
|---|---|---|---|
| | $K_1$ | $K_2$ | |
| $L$ | 8.4 | 4.5 | 1.87 |
| $R_i$ | 8.2 | 4.8 | 1.71 |
| $k_p$ | 12.3 | 2.7 | 4.56 |
| $S_0$ | 8.4 | 4.5 | 1.87 |
| $\mu$ | 4.7 | 8.2 | 1.74 |

Darcy's law for single-phase flow is used in the model, and as such the model is only applicable to the wells with very low or very high water cut level. The model validation using the field data from a shallow sandstone reservoir in Kazakhstan showed that the model could predict sanding behavior with maximum error of 5%–20% at the early development stage of most wells, but fails at later stage when the water cut value would change significantly and the flow would be multiphase instead of single-phase flow as in the original assumption. Despite the above limitations, the proposed model would be yet valuable to assess the sanding potential for the production from new wells in the local regions of Kazakhstan with the shallow weak sandstone reservoirs and fairly homogeneous rock structure as its performance has been proven in these circumstances.

## 6. Conclusions

In this study, a prediction model was developed to estimate the sand volume produced from weak sandstone formations in Kazakhstan where the wellbores are cased and perforated. The failure of the horizontal perforation tunnels was modeled by taking into account stress distribution and shear failure and this defined the boundaries of the plastic zone formed around the cavity. The produced sand was estimated as the volume of the plastic zone in the shape of a wormhole as it was also observed in other laboratory studies on sand production in weak heavy oil reservoirs. The model was simple but yet did not consider material strength degradation with the sandstone that was assumed to be homogeneous and isotropic. Nevertheless, it was successful in the prediction of sand volume produced from a shallow reservoir in Kazakhstan. Sand volumes produced in different stages with sequentially increasing flow rates were predicted accurately within 5%–20% of the measured sand volumes in the field. Sensitivity analysis results indicated that the permeability of the plastic zone is the most significant factor affecting the prediction results and this requires further experimental studies on the phenomenon. The proposed model can serve as a convenient and useful tool to assist in the effective management of the local oilfields in Kazakhstan where sand production has consistently been a challenging problem. It is likely that the prediction tool can not only lead to better disposal planning of the produced sand to prevent environmental problem, but also assist in the maintenance organization to avoid drastic interruption to the production schedule.

## Conflicts of interest

The authors wish to confirm that there are no known conflicts of interest associated with this publication and there has been no significant financial support for this work that could have influenced its outcome.

## Acknowledgement

This research was sponsored by a Nazarbayev University research grant. The authors thank the operating company for the provided field data.

## Nomenclatures

| | |
|---|---|
| $a$ | Transformation angle around the $z$-axis |
| $D$ | Range value for sensitivity analysis |
| $h$ | Thickness of producing zone |
| $i$ | Transformation angle around the $y$-axis |
| $k$ | Permeability of reservoir |
| $k_p$ | Permeability of plastic zone |
| $K_1$, $K_2$ | Average of four values of the sand volume for Levels 1 and 2, respectively |
| $L$ | Perforation length |
| $m_f$ | Sand mass from fractured zone |
| $m_p$ | Sand mass from plastic zone |
| $m_{perf}$ | Sand mass from perforations |
| $m_{rf}$ | Sand mass from real field data |
| $n$ | Coefficient for permeability of plastic zone |
| $N$ | Number of perforations |
| $p_o$ | Fluid pressure at boundary |
| $p_{wf}$ | Fluid pressure at wellbore wall |
| $q$ | Flow rate |
| $r_e$ | Radius of outer boundary |
| $r_w$ | Well radius |
| $R_f$ | Radius of fractured zone |
| $R_i$ | Radius of perforation tunnel |
| $R_o$ | Radius of outer boundary for perforation tunnel |
| $R_p$ | Radius of plastic zone |
| $S$ | Skin factor |
| $S_0$ | Inherent shear strength |
| $\alpha$ | Failure angle |
| $\Sigma$ | Stress term in Mohr-Coulomb failure criterion |
| $\theta$ | Azimuth angle around borehole axis |
| $\mu$ | Fluid viscosity |
| $\nu_{fr}$ | Poisson's ratio |
| $\rho_s$ | Density of sand grains |
| $\sigma'_1$ | Effective maximum principal stress |
| $\sigma'_3$ | Effective minimum principal stress |
| $\sigma_h$ | Minimum horizontal stress |
| $\sigma_H$ | Maximum horizontal stress |

| | |
|---|---|
| $\sigma_r$ | Radial stress at distance $r$ |
| $\sigma'_r$ | Effective radial stress |
| $\sigma^o_x, \sigma^o_y$ | Principal normal stresses at outer boundary in $x$ and $y$ directions, respectively |
| $\sigma_a$ | Axial stress |
| $\sigma^o_z$ | Axial stress at outer boundary |
| $\sigma_\theta$ | Tangential stress |
| $\tau^o_{xy}$ | Tangential stress at outer boundary |
| $\phi$ | Porosity of reservoir |

## References


Al-Shaaibi SK, Al-Ajmi AM, Al-Wahaibi Y. Three dimensional modeling for predicting sand production. Journal of Petroleum Science and Engineering 2013;109:348–63.

Araujo-Guerrero EF, Alzate GA, Arbelaez-Londono A, Pena S, Cardona A, Naranjo A. Analytical prediction model of sand production integrating geomechanics for open hole and cased–perforated wells. In: SPE heavy and extra heavy oil conference. Society of Petroleum Engineers (SPE); 2014. https://doi.org/10.2118/171107-MS.

Bradford IDR, Cook JM. A semi-analytic elastoplastic model for wellbore stability with applications to sanding. In: Rock mechanics in petroleum engineering. SPE; 1994. p. 347–54. https://doi.org/10.2118/28070-MS.

Bratli RK, Risnes R. Stability and failure of sand arches. SPE Journal 1981;21(2):236–48.

Charlez PA. Rock mechanics: petroleum applications. Editions Technip; 1997.

Dake LP. Fundamentals of reservoir engineering. New impression edition. Elsevier; 1983.

Fjær E, Holt RM, Horsrud P, Raaen AM, Risnes R. Petroleum related rock mechanics. 2nd ed. Elsevier; 2008.

Geilikman MB, Dusseault MB, Dullien FA. Sand production as a viscoplastic granular flow. In: SPE formation damage control symposium. SPE; 1994. https://doi.org/10.2118/27343-MS.

Gholami R, Aadnoy B, Rasouli V, Fakhari N. An analytical model to predict the volume of sand during drilling and production. Journal of Rock Mechanics and Geotechnical Engineering 2016;8(4):521–32.

Goshtasbi K, Elyasi A, Naeimipour A. Numerical assessment of the mechanical stability in vertical, directional and horizontal wellbores. International Journal of Mining Science and Technology 2013;23(6):937–42.

Hayavi MT, Abdideh M. Establishment of tensile failure induced sanding onset prediction models for cased-perforated gas wells. Journal of Rock Mechanics and Geotechnical Engineering 2017;9(2):260–6.

Jin Y, Chen KP, Chen M. Development of tensile stress near a wellbore in radial porous media flows of high pressure gas. International Journal of Rock Mechanics and Mining Sciences 2011;48(8):1313–9.

Morita N, Whitfill DL, Fedde OP, Levik TH. Parametric study of sand-production prediction: analytical approach. SPE Production Engineering 1989;4(1):25–33.

Nouri A, Vaziri H, Belhaj H, Islam M. Sand-production prediction: a new set of criteria for modeling based on large-scale transient experiments and numerical investigation. SPE Journal 2006;11(2):26–9.

Papamichos E, Furui E. Sand production initiation criteria and their validation. In: 47th US rock mechanics/geomechanics symposium. American Rock Mechanics Association (ARMA); 2013. p. 198–206.

Risnes R, Bratli RK, Horsrud P. Sand stresses around a wellbore. Society of Petroleum Engineers Journal 1982;22(6):883–98.

Taguchi G, Rafanelli AJ. Taguchi on robust technology development: bringing quality engineering upstream. ASME Press; 1993.

Tremblay B, Sedgwick G, Vu D. A review of cold production in heavy oil reservoirs. In: IOR 1999 – 10th european symposium on improved oil recovery. European Association of Geoscientists and Engineers (EAGE); 1999.

Tronvoll J, Fjær E. Experimental study of sand production from perforation cavities. International Journal of Rock Mechanics and Mining Sciences and Geomechanics Abstracts 1994;31(5):393–410.

van den Hoek PJ, Geilikman MB. Prediction of sand production rate in oil and gas reservoirs. In: SPE annual technical conference and exhibition. SPE; 2003. https://doi.org/10.2118/84496-MS.

Worden RH, Morad S. Clay minerals in sandstones: controls on formation, distribution and evolution. In: Worden RH, Morad S, editors. Clay mineral in sandstones. International Association of Sedimentologists; 2003. p. 1–41.

Yi X, Valko PP, Russell JE. Effect of rock strength criterion on the predicted onset of sand production. International Journal of Geomechanics 2005;5(1):66–73.


**Ainash Shabdirova** is a PhD candidate at the School of Engineering of Nazarbayev University, Kazakhstan. She obtained her BSc degree from Kazakh-British Technical University, Almaty, Kazakhstan, and MSc degree from Heriot-Watt University, Edinburgh, UK. She worked as a scientist in the research institute of a national oil company before starting her graduate studies and has worked as a research assistant on sand production related research project.

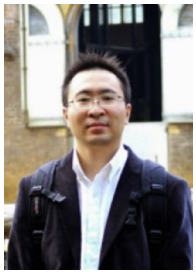

**Dr. Nguyen Hop Minh** is a faculty member at Fulbright University Vietnam, a new innovative liberal arts and engineering university established by the governments of the USA and Vietnam. He conducts research in different countries from Europe to Asia and publishes in the area of soils and soft rock behavior with applications in geotechnical engineering and hydrocarbon reservoir engineering. He is a member of a research group focusing on the micro to macro soil mechanics in UK. Dr. Nguyen Hop Minh has good experiences in startup universities where he developed new engineering curriculum, established research agenda and built research laboratories from scratch with funding from both academia and industry.

**Dr. Yong Zhao** is a professor of Mechanical Engineering in the School of Engineering, Nazarbayev University, Kazakhstan. His research interests include computational fluid, structure interaction, and multi-scale and multi-physics simulations.